Scientific Publications

World Journal of Geomatics and Geosciences, 2026, 5, 6669
www.scipublications.com/journal/wjgg
DOI: 10.31586/wjgg.2026.6669

Article

Assessment of Shoreline Deformation Using InSAR and DSAS along the San Bartholomeo River, Niger Delta, Nigeria

Horsfall Isikima Ibiwari [1], Lawrence Hart [1,*], Tamunobelema Oba [1]

[1] Department of Surveying and Geomatics, Rivers State University, Port Harcourt, Nigeria

*Correspondence: Lawrence Hart (lawrence.hart@ust.edu.ng)

Abstract: This study investigates the spatial and temporal dynamics of shoreline deformation along the San Bartholomeo River over 30 years (1995–2025) using an integrated geospatial approach. The research combines Interferometric Synthetic Aperture Radar (InSAR) and Digital Shoreline Analysis System (DSAS) techniques to quantify both vertical land motion and horizontal shoreline change. Results reveal a decline in land area from 32.622 km² (56.65%) in 1995 to 30.284 km² (52.59%) in 2025, alongside an increase in water body extent, indicating progressive shoreline retreat. Shoreline change rates varied significantly, with erosion reaching −8.04 m/yr and accretion up to 16.73 m/yr. Net Shoreline Movement (NSM) and Shoreline Change Envelope (SCE) analyses further highlighted zones of persistent erosion and high variability. InSAR-derived deformation patterns confirmed the presence of subsidence contributing to shoreline instability. The findings demonstrate that a combination of hydrodynamic forces, sediment imbalance, and anthropogenic activities drives shoreline deformation in the study area. This study contributes to improved shoreline monitoring by integrating vertical and horizontal deformation metrics, providing a robust framework for sustainable shoreline management in deltaic environments.

Keywords: Shoreline Deformation, InSAR, DSAS, Erosion, Subsidence, Shoreline Dynamics

How to cite this paper:
Ibiwari, H. I., Hart, L., & Oba, T. (2026). Assessment of Shoreline Deformation Using InSAR and DSAS along the San Bartholomeo River, Niger Delta, Nigeria. *World Journal of Geomatics and Geosciences, 5*(1), 11-25.
DOI: 10.31586/wjgg.2026.6669

Received: June 28, 2026
Revised: August 9, 2026
Accepted: August 27, 2026
Published: September 1, 2026

1. Introduction

Shorelines represent dynamic boundaries that continuously respond to environmental forcing and human activities. In deltaic environments such as the Niger Delta, shoreline deformation poses significant risks to ecosystems, infrastructure, and local livelihoods. Increasing pressures from climate variability, sediment disruption, and anthropogenic activities have intensified shoreline instability, making accurate monitoring essential (Odunuga, Oyebande, Omojola, & Adeaga, 2015; Ndubisi & Ezirim, 2021) [1,2].

Traditional shoreline studies have largely focused on horizontal movement using optical imagery, often neglecting vertical land motion such as subsidence. However, recent advances in satellite geodesy, particularly Interferometric Synthetic Aperture Radar (InSAR), have enabled the detection of millimetre-scale ground deformation, offering new opportunities for integrated shoreline analysis. Previous studies (Vousdoukas et al., 2020; Cooper & Pontee, 2016) [3,4] emphasize the importance of monitoring shoreline change using geospatial techniques. However, many studies neglect vertical deformation. Despite the growing application of geospatial technologies in coastal monitoring, no published study has comprehensively assessed shoreline deformation along the San Bartholomeo River using an integrated InSAR and Digital Shoreline Analysis System (DSAS) approach. Existing studies have established that coastal and shoreline terrain can be monitored using conventional techniques with sparse and discrete spatial information. However, the knowledge gap has heightened the quest for the availability of reliable spatial information needed to understand long-term shoreline dynamics and to support evidence-based coastal management in the area. Addressing this issue is critical because the consequences of coastal and shoreline changes will impact the socioeconomic realities of the communities and critical investments of operating companies in the location. Given this identified gap, this study integrates Interferometric Synthetic Aperture Radar (InSAR) and DSAS-derived shoreline metrics to assess shoreline deformation in the San Bartholomeo River, a riverine–mangrove system in the Niger Delta where persistent shoreline instability threatens coastal ecosystems, infrastructure, and the livelihoods of adjoining communities. Specifically, the study quantifies the rate, magnitude, and spatial extent of shoreline deformation over 30 years (1995–2025) using InSAR observations and DSAS statistical models. The findings provide baseline geospatial information to support sustainable shoreline management, climate adaptation, disaster-risk reduction, and coastal resilience planning in the Niger Delta.

2. Study Area

The study is located in Akuku-Toru Local Government Area of Rivers State, in the Niger Delta region of Nigeria. The area is a stretch along the San Bartholomeo River, characterized by low-lying terrain, tidal influence, mangrove vegetation, and unconsolidated sediments. These features make the shoreline highly susceptible to erosion, accretion, and subsidence. It has a shoreline that stretches approximately 41km in length and spans from a point at Ekulama I on Latitude 4° 33′ 44″ N and Longitude 6° 42′ 46″ E to Ekulama II on Latitude 4° 32′ 55″ N and Longitude 6° 39′ 46″ E. Ezekwe, Eludoyin, and Adigwu (2015) [5] explained that the area is among the swampiest of the ecological zones, under tidal influence. The vegetation around the river consists of a mangrove system intermingled with rainforest. As depicted in Figure 1, the river is economically important to Rivers State and Nigeria at large, as it hosts major flow stations, such as Ekulama I and II, which provide gas feedback to the Nigerian government-owned Bonny LNG terminal (Ezekwe et al., 2015) [5].

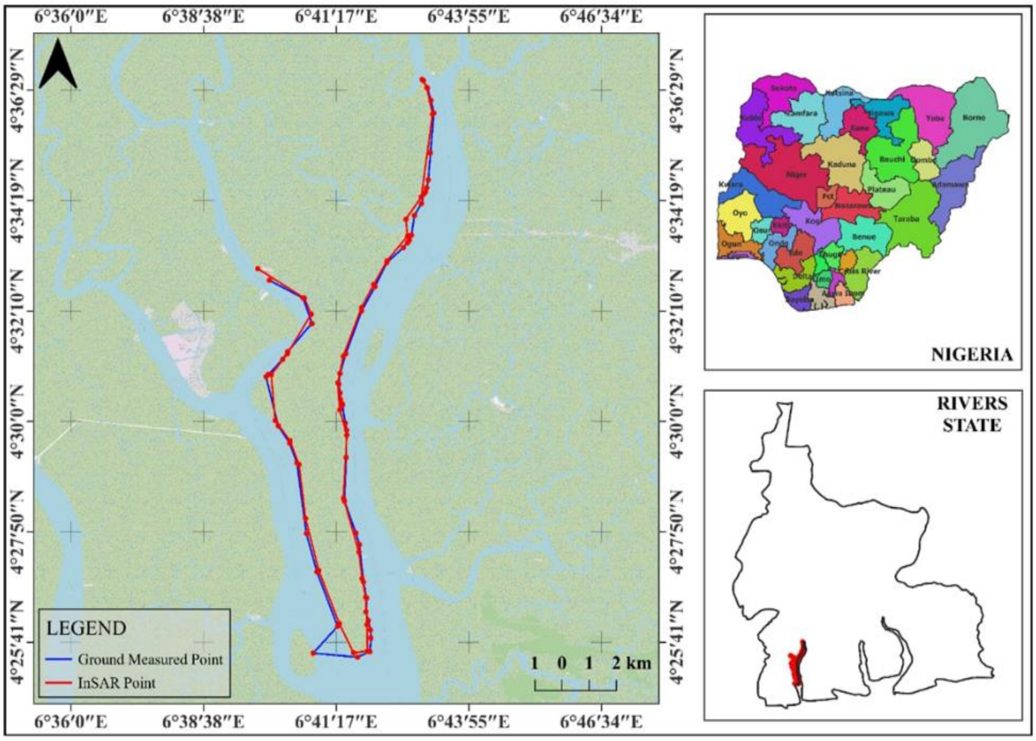

Figure 1. Map of the Study Area showing its Stretch

3. Materials and Methods

This research adopts an integrated remote sensing and Interferometric Synthetic Aperture Radar (InSAR) methodological framework to assess shoreline deformation and vertical land motion along the San Bartholomeo River. It uses a quantitative approach. Quantitative because it deals with measurable changes in shoreline position, erosion, accretion, and subsidence, and uses statistical analysis to achieve the research objectives.

3.1. InSAR Radar Data

Multi-temporal Synthetic Aperture Radar (SAR) images from satellites such as Sentinel-1, Radarsat-1, and Radarsat-2 provide raw interferometric phase data for deformation analysis. The research used satellite imagery from four distinct years (1995, 2005, 2015, and 2025) to create a comprehensive temporal dataset of shoreline changes. The selected years correspond to key periods of interest, with each dataset providing insights into both short-term and long-term shoreline dynamics. In Synthetic Aperture Radar (SAR), a satellite transmits a microwave signal toward the Earth's surface. The signal is reflected, and the satellite records the returned wave. The Radar Signal can be represented as:

$$S = Ae^{i\o} \quad (1)$$

Where:
S = Complex Radar Signal
A = amplitude (depends on surface roughness, dielectric properties, etc.)
ϕ= phase of the radar signal
e = exponential operator representing wave behavior
i = imaginary unit, allowing 2D representation (cos + sin)
The phase is directly related to the distance between the radar and the ground target:

$$\phi = \frac{4\pi R}{\lambda} \quad (2)$$

Where:
R = range (satellite-to-ground distance)
λ = radar wavelength

3.2. Data Acquisition

Table 1. Showing List of Data Acquisition Sources

Year	Satellite	Sensor	Resolution	Data Source
1995	Radarsat-1	Synthetic Aperture Radar (SAR)	25 m (nominal)	CSA
2005	Radarsat-2	Synthetic Aperture Radar (SAR)	20 m (nominal)	CSA
2015	Sentinel -1	Synthetic Aperture Radar (SAR)	10 m (nominal)	ESA
2025	Sentinel -1	Synthetic Aperture Radar (SAR)	10 m (nominal)	ESA

Note. SAR = Synthetic Aperture Radar; CSA = Canadian Space Agency; ESA = European Space Agency.

3.3. Data Analysis

The raw Sentinel-1 SAR data were imported into SNAP software (Sentinel Application Platform) using the Read function, which loaded the satellite images required for further processing. InSAR processing was carried out using SNAP software to derive vertical land motion. Time-series techniques (e.g., SBAS/PSI were used to estimate deformation rates. Once the data were loaded, the next step involved generating the interferogram by comparing the phase differences between two SAR images captured at different times. This interferogram highlighted any displacement of the Earth's surface between the two acquisition dates, providing the fundamental data for understanding shoreline deformation. Since the Sentinel-1 data is acquired in TOPSAR mode (which divides the data into multiple sub-swaths or bursts), the TOPSAR-Deburst process was applied to split the data into individual sub-swaths, allowing for more accurate and efficient analysis of the area of interest (AOI) and reducing unnecessary data.

3.4. Shoreline Extraction and Analysis

Shorelines were extracted from satellite imagery and analysed using DSAS. Key metrics include:

3.4.1. Endpoint Rate (EPR)

The EPR measures the rate of shoreline change by directly comparing the positions of the shoreline between two time periods (e.g., 1995–2005, 2005–2015, and 2015–2025). The EPR is calculated by dividing the distance between the shoreline positions at the two endpoints by the time difference.

Endpoint Rate (EPR):

$$\frac{Distance}{Time} = \frac{E-B}{T} \tag{3}$$

Where:
E = Endpoint
B = Beginning Point

The EPR provides a simple but effective measure of the rate of shoreline movement, particularly for cases where only two points (beginning and end of the period) are available. It gives a clear snapshot of how fast the shoreline has changed over the time period in question.

3.4.2. Linear Regression Rate (LRR)

The LRR method uses a least squares regression to determine the best-fit line through the shoreline positions at each transect over time. The slope of this line represents the rate of shoreline change per year. The LRR provides a smoothed estimate of the rate of change, accounting for long-term trends in shoreline movement. It is particularly useful when there are multiple data points (e.g., multiple years) and when the shoreline has experienced fluctuating changes over time. In this study, the DSAS tool was used in ArcGIS. It is calculated for each transect between the selected years (1995–2005, 2005–2015, and 2015–2025). LRR is typically expressed in meters per year (m/yr). Mathematically, it is given as:

$$L = mx + b \tag{4}$$

Where:
L = The shoreline position (distance in meters, from a set baseline)
x = The date of the shoreline survey (years)
m = The calculated linear regression rate of change (slope/rate)
b = The estimated y-intercept of the regression line.

3.4.3. Net Shoreline Movement (NSM)

The NSM measures the total distance between the oldest and most recent shoreline positions along each transect. It provides a direct measure of long-term shoreline displacement, indicating whether a particular section has experienced net erosion or net accretion over the study period. Mathematically, NSM is expressed as:

$$NSM = S_{final} - S_{inital} \tag{5}$$

Where:

S_{final} = most recent shoreline position
S_{inital}= earliest shoreline position

3.4.4. Shoreline Change Envelope (SCE)

Shoreline Change Envelope measures the total range of shoreline movement, defined as the distance between the most landward and most seaward shoreline positions recorded across all time periods. It is expressed mathematically as:

$$SCE = S_{max} - S_{min} \quad (6)$$

Where:
S_{max} = most seaward shoreline position
S_{min} = most landward shoreline position

3.5. Validation

To ensure the reliability of the InSAR-derived results, a validation exercise was conducted as a crucial part of this research. It was done to verify satellite-based measurements of shoreline deformation by comparing them with on-the-ground observations. The difference between ground-measured height and InSAR-derived height was computed to assess accuracy. The height difference computation is given as;

$$\Delta h = h_{InSAR} - h_{Ground} \quad (7)$$

Where:
Δh = difference between InSAR-derived height and ground-measured height
h_{InSAR} = InSAR-derived vertical displacement
h_{Ground} = Ground control measured height

3.6. Statistical Analyses

The validated ground data were integrated into the overall analysis to enhance the interpretation of the deformation patterns. Statistical analysis plays a critical role in evaluating the accuracy and reliability of geospatial datasets, particularly in deformation monitoring using InSAR and ground-based measurements. The use of Root Mean Square Error (RMSE) and other statistical indicators, such as Mean Absolute Error (MAE) and Correlation Coefficient, is essential for validating the consistency between observed and derived measurements. The Root Mean Square Error was computed to measure the square root of the average squared differences between values predicted by InSAR-derived heights and values observed from ground control points. This is given as:

$$RMSE = \frac{\sqrt{\Sigma(h_{InSAR} - h_{Ground})^2}}{n} \quad (8)$$

Where:
RMSE = Root Mean Square Error
h_{InSAR} = InSAR-derived vertical displacement
h_{Ground} = Ground control measured height
n = No of points

While Mean Absolute Error (MAE) was computed to measure the average absolute difference between InSAR-derived height and observed values without squaring the errors. This is given as:

$$MAE = \frac{\sqrt{\Sigma h_{InSAR} - h_{Ground}}}{n} \quad (9)$$

MAE = Mean Absolute Error
h_{InSAR} = InSAR-derived vertical displacement

h_{Ground} = Ground-measured height
n = No of points

On the other hand, the Correlation Coefficient was computed to measure the strength and direction of the linear relationship between ground-measured values and InSAR-derived values. It determines how strongly the two datasets are related. A high correlation coefficient indicates that InSAR results closely follow ground observations. It is given as:

$$r = \frac{n(\sum xy)-(\sum x)(\sum y)}{\sqrt{[n\sum x^2-(\sum x)^2][n\sum y^2-(\sum y)^2]}} \quad (10)$$

Where:
r = correlation coefficient,
n = no of points
$\sum xy$ = Sum of each x-value multiplied by its corresponding y-value
$\sum x$, $\sum y$ = the sums of each variable
$\sum x^2$, $\sum y^2$ = the sums of squared values
This implies that when r ranges from -1(perfect negative) to +1(perfect positive), it is good.

4. Results and Discussion of Findings

The results contain tables showing the extent, rate, and magnitude of shoreline deformation

Table 2. Evaluation of the Extent of Shoreline Deformation along the Study Area

Chainages	Shoreline Elevation (m)				Subsidence Change (m)		
	Z_1995	Z_2005	Z_2015	Z_2025	1995-2005	2005-2015	2015-2025
0+0000	26.991	34.026	23.468	23.477	-7.036	10.558	-0.009
0+1000	30.235	32.328	29.208	29.170	-2.093	3.120	0.038
0+2000	35.012	36.789	34.291	33.957	-1.777	2.498	0.334
0+3000	27.722	34.066	24.562	24.540	-6.343	9.504	0.022
0+4000	29.056	20.426	33.134	33.609	8.631	-12.708	-0.475
0+5000	24.906	19.071	27.835	27.811	5.835	-8.764	0.024
0+6000	27.838	18.182	32.696	32.636	9.656	-14.514	0.061
0+7000	33.016	46.827	26.128	26.094	-13.811	20.699	0.034
0+8000	25.435	29.435	23.423	23.370	-4.026	6.012	0.053
0+9000	30.168	31.334	29.530	29.641	-1.166	1.804	-0.111
1+0000	30.127	31.310	29.532	29.538	-1.183	1.778	-0.006
1+1000	35.178	22.995	41.104	41.436	12.183	-18.109	-0.332
1+2000	31.506	29.127	32.675	32.717	2.380	-3.548	-0.042
1+3000	28.744	30.192	27.988	28.052	-1.448	2.204	-0.064
1+4000	26.787	28.111	26.143	26.107	-1.324	1.967	0.037
1+5000	25.739	29.495	23.862	23.862	-3.756	5.633	0.000
1+6000	27.179	28.954	26.217	26.367	-1.775	2.737	-0.150
1+7000	29.071	30.194	28.477	28.542	-1.123	1.717	-0.065
1+8000	26.951	28.076	26.210	26.568	-1.125	1.866	-0.359
1+9000	25.112	19.487	28.006	27.844	5.626	-8.520	0.162
2+0000	28.530	19.000	33.295	33.295	9.530	-14.295	0.000
2+1000	23.820	19.065	26.208	26.186	4.755	-7.143	0.022

2+2000	24.692	18.861	27.751	27.464	5.831	-8.890	0.287
2+3000	26.701	30.007	25.049	25.046	-3.306	4.958	0.002
2+4000	28.675	19.859	33.226	32.940	8.816	-13.367	0.286
2+5000	25.624	19.371	28.522	28.979	6.253	-9.150	-0.457
2+6000	27.945	31.041	26.391	26.405	-3.095	4.650	-0.014
2+7000	25.143	24.347	25.598	25.483	0.796	-1.251	0.116
2+8000	25.884	23.380	27.073	27.200	2.504	-3.693	-0.127
2+9000	25.130	18.759	28.442	28.189	6.371	-9.683	0.253
3+0000	27.181	28.818	26.499	26.226	-1.637	2.319	0.273
3+1000	27.039	28.392	26.428	26.297	-1.353	1.964	0.131
3+2000	30.892	34.132	29.083	29.461	-3.240	5.049	-0.377
3+3000	25.092	20.750	27.138	27.388	4.342	-6.388	-0.250
3+4000	24.801	28.109	23.128	23.165	-3.309	4.981	-0.036
3+5000	23.437	24.209	23.086	23.016	-0.772	1.124	0.070
3+6000	24.650	26.295	23.877	23.778	-1.645	2.418	0.098
3+7000	24.299	24.218	24.376	24.304	0.081	-0.158	0.073
3+8000	28.137	28.560	28.019	27.832	-0.423	0.541	0.187
3+9000	24.140	25.012	23.706	23.702	-0.872	1.306	0.004
4+0000	22.032	20.051	23.014	23.030	1.981	-2.963	-0.017
4+0178	24.757	22.002	26.135	26.135	2.755	-4.133	0.001

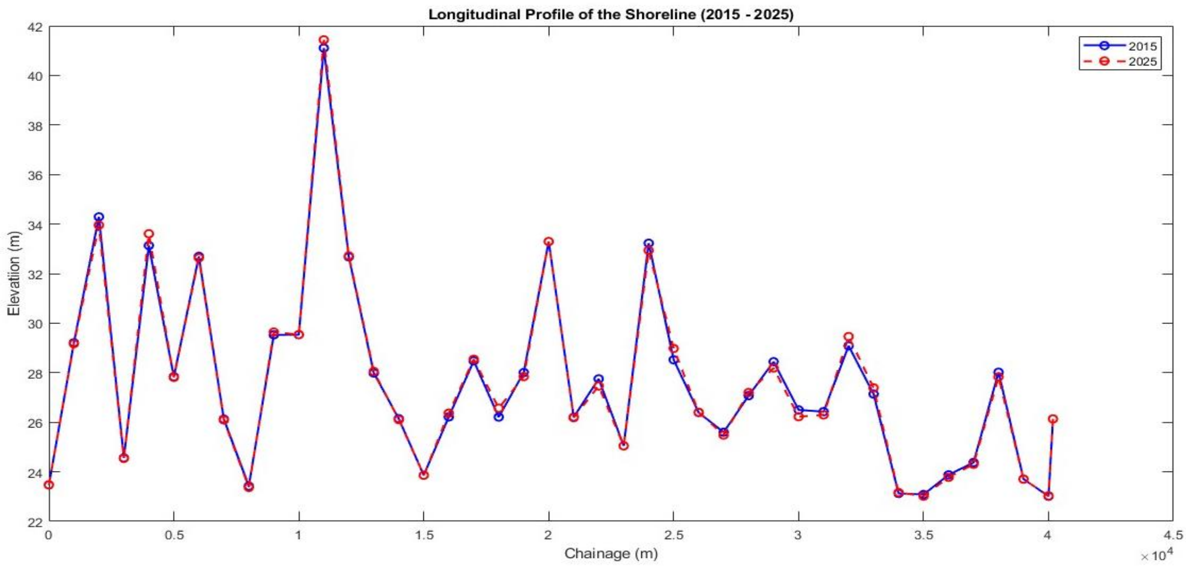

Figure 2. Evaluation of the Extent of Shoreline Deformation Between 2015 and 2025

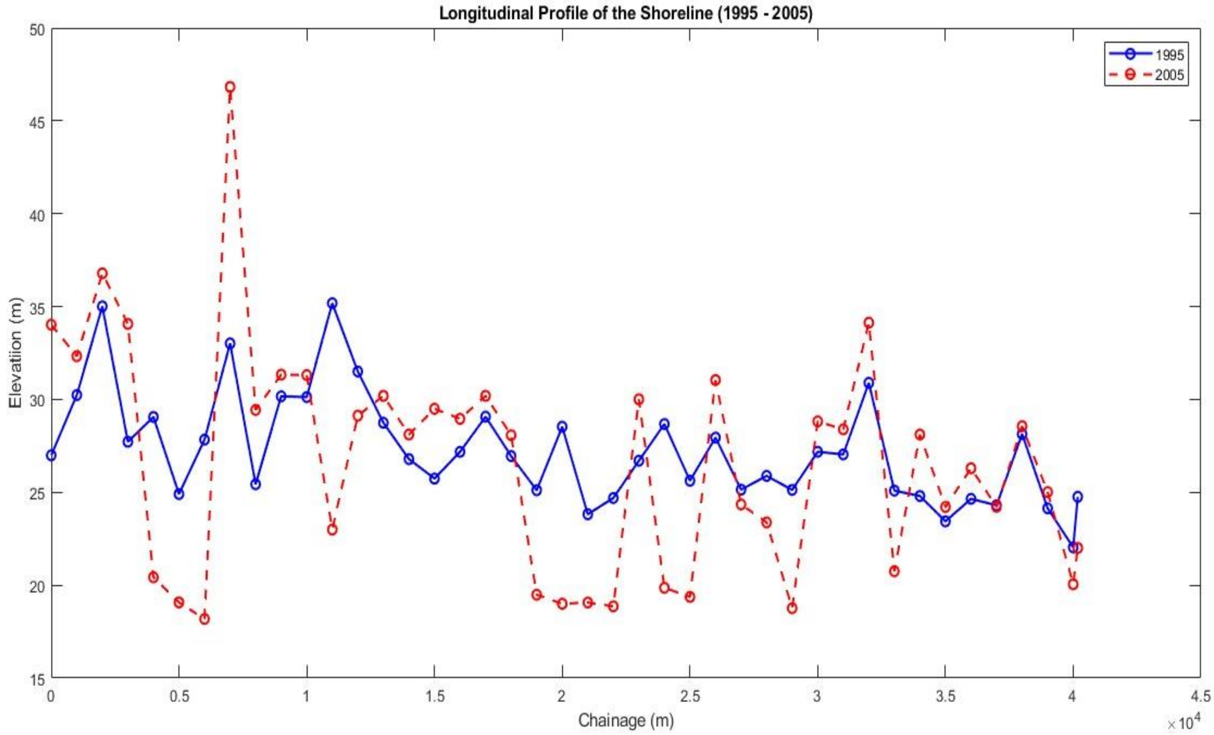

Figure 3. Evaluation of the Extent of Shoreline Deformation Between 1995 and 2005

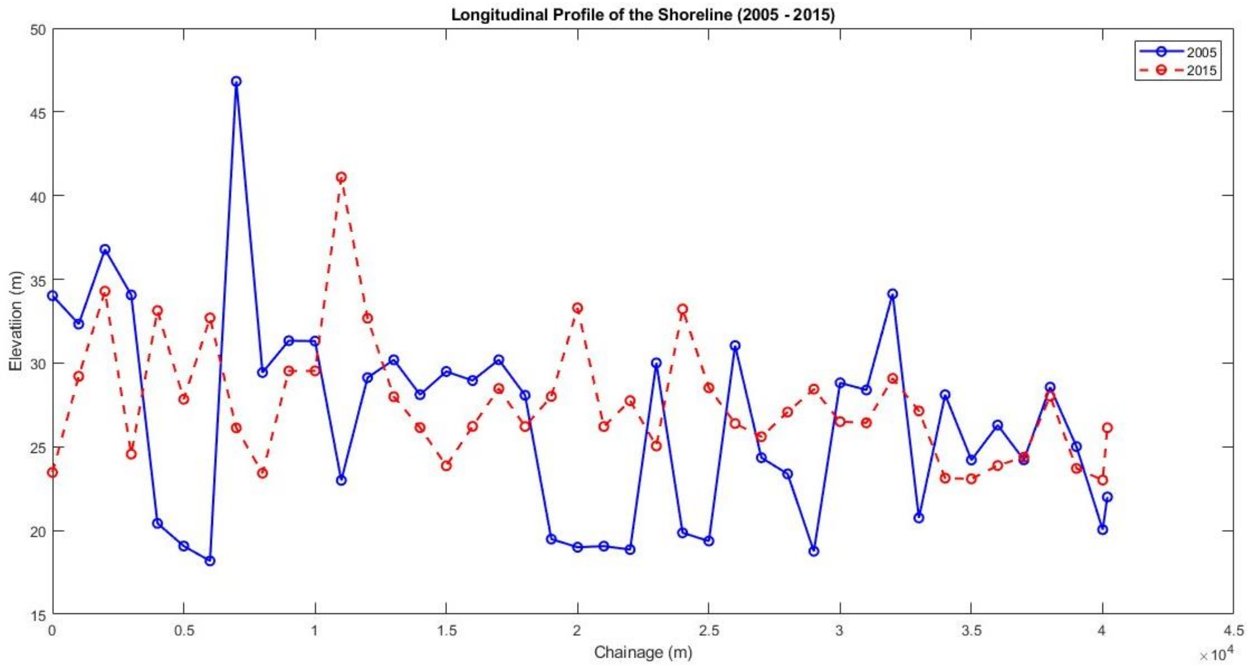

Figure 4. Evaluation of the Extent of Shoreline Deformation Between 2005 and 2015

4.1. Rate and Magnitude of Shoreline Deformation

Shoreline change rates varied significantly across transects:

Table 3. Evaluation of Rate of Shoreline Deformation

Transect Order	Linear Regression Rate (LRR) (m/yr)	End Point Rate (EPR) (m/yr)	Net Shoreline Movement (NSM) (m/yr)	Shoreline Change Envelope (SCE) (m/yr)
1	-8.04	-8.04	-160.74	-160.74
2	-6.04	-6.04	-120.81	-120.81
3	-1.11	-1.11	-22.15	-101.43
4	-3.94	-3.94	-78.74	-114.81
5	-2.37	-2.37	-47.33	-90.55
6	-1.42	-1.42	-28.34	-46.11
7	-2.37	-2.37	-47.46	-51.05
8	-1.49	-1.49	-29.78	-29.78
9	-4.59	-4.59	-91.90	-155.52
10	-7.60	-7.13	-213.80	-253.36
11	-9.91	-9.90	-296.97	-308.17
12	-8.63	-8.63	-172.50	-172.50
13	-4.78	-4.78	-95.53	-120.19
14	-1.67	-1.67	-33.31	-33.31
15	-3.91	-3.68	-110.53	-110.53
16	-4.73	-4.73	-94.55	-94.55
17	2.50	2.79	83.70	83.70
18	-2.20	-2.36	-70.72	-74.85
19	-4.64	-6.06	-181.92	-181.92
20	6.14	7.15	214.44	216.8
21	5.50	5.30	158.99	195.85
22	6.80	7.94	238.10	262.91
23	5.23	5.90	177.07	237.75
24	-1.77	-1.45	-43.35	-96.90
25	3.31	1.65	49.39	182.65
26	8.82	8.62	258.52	353.44
27	16.06	16.73	501.86	577.76
28	17.80	18.74	562.28	677.71
29	14.58	16.69	500.71	586.29
30	5.53	6.40	192.01	272.08
31	0	-2.00	-20.03	-20.03
32	-4.80	-5.23	-156.93	-156.93
33	13.14	15.01	450.34	495.28
34	17.57	19.49	584.84	625.78
35	18.97	20.54	616.05	736.09

NSM analysis revealed cumulative shoreline retreat in several transects, while SCE indicated high variability in shoreline positions, reflecting dynamic sediment processes.

4.2. Vertical Land Motion (InSAR Results)

InSAR analysis identified zones of subsidence, which correlate with areas of high shoreline retreat. This confirms that vertical deformation contributes significantly to shoreline instability.

Maximum erosion: **−8.04 m/yr**

Maximum accretion: **16.73 m/yr**

Table 4. Evaluation of Magnitude of Shoreline Deformation

Magnitude Class	EPR Range (m/yr)	Interpretation
Very Low	0 – 1	Stable shoreline
Low	>1 – 3	Slight change
Moderate	>3 – 7	Noticeable change
High	>7 – 15	Severe deformation
Very High	>15	Extreme deformation

Table 5. Coordinates and heights from InSAR-derived and Ground Points

Point ID	**Ground**		**Ellipsoidal Height**	**InSAR**		**Ellipsoidal Height**
	Easting(m)	Northing(m)		Easting(m)	Northing(m)	
1	241010.360	502899.750	23.208	240582.791	503322.661	23.477
2	242245.560	502259.030	33.641	242294.139	502253.936	33.957
3	242554.920	501327.620	24.317	242547.890	501675.539	24.540
4	241676.770	500325.450	28.010	241661.679	500244.919	27.811
5	241494.970	500049.460	32.798	241066.082	499496.142	32.636
6	241319.890	497648.500	23.107	241208.747	497840.280	23.370
7	241736.380	497024.190	28.924	241750.156	497109.033	29.641
8	242003.000	496308.580	29.919	242077.568	496248.677	29.538
9	242341.990	493764.830	32.019	242314.933	494302.113	32.717
10	242728.380	492374.550	25.914	242794.444	492422.716	26.107
11	243483.800	490408.410	25.644	243546.088	490505.758	26.367
12	244213.950	489291.640	29.221	244067.646	489453.612	28.542
13	244669.520	489492.310	26.202	244579.364	489509.009	26.568
14	244610.950	490617.710	27.745	244566.901	490459.240	27.844
15	244439.490	492002.560	26.514	244392.850	492127.872	26.186
16	244292.310	493358.430	27.404	244276.285	493090.085	27.464
17	243747.510	494926.820	33.001	243712.605	495033.493	32.940
18	243837.220	497489.290	26.497	243842.578	497306.878	26.405
19	243675.520	498446.300	25.509	243588.512	498220.666	25.483
20	243555.860	499146.510	26.894	243521.318	499192.941	27.200
21	243816.450	500244.810	28.815	243721.905	500150.821	28.189
22	244403.670	501785.030	26.312	244398.717	501904.788	26.297
23	244896.010	502658.150	29.815	244849.221	502738.193	29.461
24	245332.890	503523.610	27.107	245350.387	503598.195	27.388
25	246244.320	504509.520	23.479	246102.447	504481.309	23.165

26	246361.120	505227.300	23.104	246043.347	505091.989	23.016
27	246715.020	506005.950	23.800	246615.432	505892.653	23.778
28	247087.390	508916.580	23.585	247037.020	508874.116	23.702
29	246850.100	509824.770	23.188	246832.776	509831.155	23.030
30	246657.770	510130.240	25.914	246704.000	510092.758	26.135

4.3. Statistical Accuracy Assessment

To validate the agreement between the datasets, some statistical analyses were performed: Root Mean Square Error was computed using equation 8 and the correlation coefficient in equation 10.

Scientific Publications

World Journal of Geomatics and Geosciences, 2026, 5, 6669
www.scipublications.com/journal/wjgg
DOI: 10.31586/wjgg.2026.6669

Table 6. Statistical Accuracy Assessment

	GROUND				INSAR									
Eastings	**Northings**	**Ellipsoidal Height**	**∑x**	**Eastings**	**Northings**	**Ellipsoidal Height**	**∑y**	**Difference**	**Sum**	**SumSq**	**SqRT**	**RMSE**	**Cor. Coeff**	
241010.360	502899.750	23.208	843.501	240582.791	503322.661	23.477	846.249	0.269	2.748	5.639368	2.374735	0.077	0.992	
242245.560	502259.030	33.641		242294.139	502253.936	33.957		0.316						
242554.920	501327.620	24.317		242547.890	501675.539	24.540		0.223						
241676.770	500325.450	28.010		241661.679	500244.919	27.811		-0.199						
241494.970	500049.460	32.798		241066.082	499496.142	32.636		-0.162						
241319.890	497648.500	23.107		241208.747	497840.280	23.370		0.263						
241736.380	497024.190	28.924		241750.156	497109.033	29.641		0.717						
242003.000	496308.580	29.919		242077.568	496248.677	29.538		-0.381						
242341.990	493764.830	32.019		242314.933	494302.113	32.717		0.698						
242728.380	492374.550	25.914		242794.444	492422.716	26.107		0.193						
243483.800	490408.410	25.644		243546.088	490505.758	26.367		0.723						
244213.950	489291.640	29.221		244067.646	489453.612	28.542		-0.679						
244669.520	489492.310	26.202		244579.364	489509.009	26.568		0.366						
244610.950	490617.710	27.745		244566.901	490459.240	27.844		0.099						
244439.490	492002.560	26.514		244392.850	492127.872	26.186		-0.328						
244292.310	493358.430	27.404		244276.285	493090.085	27.464		0.060						
243747.510	494926.820	33.001		243712.605	495033.493	32.940		-0.061						
243837.220	497489.290	26.497		243842.578	497306.878	26.405		-0.092						
243675.520	498446.300	25.509		243588.512	498220.666	25.483		-0.026						
243555.860	499146.510	26.894		243521.318	499192.941	27.200		0.306						
243816.450	500244.810	28.815		243721.905	500150.821	28.189		-0.626						
244403.670	501785.030	26.312		244398.717	501904.788	26.297		-0.015						
244896.010	502658.150	29.815		244849.221	502738.193	29.461		-0.354						
245332.890	503523.610	27.107		245350.387	503598.195	27.388		0.281						
246244.320	504509.520	23.479		246102.447	504481.309	23.165		-0.314						

246361.120	505227.300	23.104	246043.347	505091.989	23.016	-0.088
246715.020	506005.950	23.800	246615.432	505892.653	23.778	-0.022
247087.390	508916.580	23.585	247037.020	508874.116	23.702	0.117
246850.100	509824.770	23.188	246832.776	509831.155	23.030	-0.158
246657.770	510130.240	25.914	246704.000	510092.758	26.135	0.221

As discussed earlier, the Correlation Coefficient was computed to measure the strength and direction of the linear relationship between ground-measured values and InSAR-derived values. It determines how strongly the two datasets are related. A high correlation coefficient indicates that InSAR results closely follow ground observations.

The correlation coefficient ranges from -1 (perfect negative) to +1 (perfect positive), so a value close to +1 is good. The result shows that a strong positive correlation existed between ground measurements and InSAR-derived displacement values, demonstrating the high reliability of the InSAR technique.

5. Discussion on Results and Findings

The results demonstrate that a combination of natural and anthropogenic factors drives shoreline deformation. Hydrodynamic forces and sediment imbalance are primary natural drivers, while human activities such as dredging and oil exploration exacerbate deformation.

The integration of InSAR and DSAS provides a more comprehensive understanding of shoreline dynamics by capturing both vertical and horizontal changes. This approach addresses limitations in previous studies that relied solely on optical data and traditional surveying methods, which are limited to horizontal changes and are costly and time-consuming.

The evaluation of shoreline deformation extent, presented in Table 3, demonstrated a combination of erosion, accretion, and subsidence across the study area. Erosion was most pronounced at chainages 0+5000 and 0+6000 in 2005, where the shoreline elevation declined significantly, whereas accretion was observed at chainages 26 and 30, with elevation increases. Subsidence was also evident, particularly in zones where the shoreline consistently sank over time. These findings are consistent with other studies on shoreline dynamics in river systems, which show that shoreline deformation often results from a combination of natural processes, including sediment transport, hydrological fluctuations, and tectonic influences (Liu, Yang, Xi, Guo, & Yang, 2023) [6]. The findings of this study highlight the varying impacts of these forces along different stretches of the San Bartholomeo River, supporting previous work on the complex nature of shoreline changes in coastal and riverine areas.

The analysis of the rate and magnitude of shoreline deformation in Table 2 and Table 3 revealed that the study area experienced both high rates of erosion and significant accretion. The Linear Regression Rate (LRR) and Endpoint Rate (EPR) indicated substantial erosion in certain areas, such as Transects 1, 2, and 9, with EPR values as low as -8.04 m/yr, while other areas, like Transects 27 and 28, showed positive rates of shoreline advance, with EPRs as high as 16.73 m/yr. The classification of deformation magnitudes further revealed that high- and very-high-deformation zones were concentrated along these transects, where the most significant changes occurred. These findings align with studies by Gornitz et al. (2020) [7], who reported similarly high rates of shoreline deformation in coastal areas, where accelerated erosion is often driven by anthropogenic factors such as land-use change and river management practices. The identification of severe and extreme deformation zones in this study underscores the importance of monitoring and addressing shoreline changes in regions experiencing high rates of erosion. This study contributes to the achievement of the United Nations Sustainable Development Goals by generating geospatial evidence to support climate adaptation, sustainable coastal management, and disaster risk reduction. Specifically, the findings advance SDG 13 (Climate Action) through improved understanding of climate-induced shoreline dynamics and anthropogenic impacts. With quantitative evidence of shoreline deformation, it identifies hotspots of erosion and accretion. This will indeed support resilient land-use planning and infrastructure development in vulnerable coastal communities.

6. Conclusion

This study provides a comprehensive assessment of shoreline deformation along the San Bartholomeo River using integrated geospatial techniques. The findings highlight the importance of combining InSAR and DSAS for accurate shoreline monitoring and support evidence-based policy and Coastal Zone Management.

7. Recommendations

1. Continuous InSAR monitoring should be implemented along the San Bartholomeo Shoreline to detect subtle changes in shoreline position and elevation. This will provide real-time data for decision-making, particularly in areas where traditional monitoring methods are impractical due to access constraints and their cost implications.
2. Subsidence can exacerbate shoreline erosion and lead to infrastructural failure. It is recommended that local authorities work with oil and gas companies to monitor subsidence risks regularly and develop mitigation strategies to safeguard critical infrastructure, such as platforms and pipelines along the shoreline.
3. Policymakers should ensure that the potential impacts of these activities on shoreline stability are carefully assessed and mitigated through stricter regulations and monitoring.

References

[1] Odunuga, S., Oyebande, L., Omojola, A. S., & Adeaga, O. (2015). Shoreline changes and their implications for urban infrastructure in coastal Lagos, Nigeria. Natural Hazards, 78(2), 1291–1308. https://doi.org/10.1007/s11069-015-1763-5

[2] Ndubisi, C.C., & Ezirim, G. E. (2021). Shoreline erosion and environmental degradation in coastal communities of Rivers State. Nigerian Journal of Environmental Sciences, 15(2), 45-58.

[3] Vousdoukas, M. I., Ranasinghe, R., Mentaschi, L., et al. (2020). Sandy coastlines under threat of erosion. Nature Climate Change, 10, 260–263. https://doi.org/10.1038/s41558-020-0697-0

[4] Cooper, J. A. G., & Pontee, N. (2016). Appraisal and evolution of the littoral 'sediment cell' concept in applied coastal management: Experiences from England and Wales. Ocean & Coastal Management, 135, 64–75. https://doi.org/10.1016/j.ocecoaman.2016.10.014

[5] Ezekwe, I.C., Eludoyin, O.S., & Adigwu, O. (2015). Land use dynamics and Mangrove Forest Decline in the Soku Oil and Gas Fields, Niger Delta Region of Nigeria. Journal of Geographic Thought & Environmental Studies, 2015, 13(1), 1-12.

[6] Liu, M., Yang, Z., Xi, W., Guo, J., & Yang, H. (2023). InSAR-based method for deformation monitoring of landslide source area in Baihetan reservoir, China. Front. Earth Sci. 11:1253272. doi: 10.3389/feart.2023.1253272.

[7] Gornitz, V., Oppenheimer, M., Kopp, R., Horton, R., Orton, P., Rosenzweig, C., Solecki, W., & Patrick, L. (2020): Enhancing New York City's resilience to sea level rise and Increased Coastal Flooding. Urban Clim., **33**, 100654, doi:10.1016/j.uclim.2020.100654.